Proceedings of ICONE23
23rd International Conference on Nuclear Engineering
May 17-21, 2015, Chiba, Japan

ICONE23-1163

CFD MODELING OF SUPERCRITICAL WATER HEAT TRANSFER IN A VERTICAL BARE TUBE UPWARD FLOW

Vladimir Agranat
Applied Computational Fluid Dynamics Analysis
Thornhill, Ontario, Canada
vlad@acfda.org

Michael Malin
Concentration, Heat & Momentum Limited
Wimbledon, London, United Kingdom
mrm@cham.co.uk

Igor Pioro
University of Ontario Institute of Technology
Oshawa, Ontario, Canada
Igor.Pioro@uoit.ca

Rand Abdullah
University of Ontario Institute of Technology
Oshawa, Ontario, Canada
Rand.Abdullah@uoit.ca

Valery A. Perminov
National Research Tomsk Polytechnic University
Tomsk, Russian Federation
valerperminov@gmail.com

ABSTRACT

A customized Computational Fluid Dynamics (CFD) model of supercritical water (SCW) heat transfer in a vertical tube upward flow is developed and partially validated using experimental data obtained under the operating conditions typical for SCW cooled reactors (SCWRs): at a pressure of 24 MPa, an inner tube diameter of 10 mm, an inlet temperature of 320 or 350 °C and a heated tube length of 4 m. The three values of mass flux (500, 1000 and 1500 kg/m^{2}s) and various values of wall heat flux (from 141 to 729 kW/m^2) are considered. Physical properties of SCW are calculated by using the REFPROP software from National Institute of Standards and Technology (NIST). The model has been incorporated into the commercial general-purpose CFD software, PHOENICS. Various turbulence models and numerical grid settings are tested. The study has demonstrated a good agreement between the CFD predictions and the experimental data on the inside tube wall temperature and heat transfer coefficient with use of a two-layer low-Reynolds-number k-ε turbulence model. However, a further model development is required under the conditions of significant effects of buoyancy force on heat transfer characteristics (the conditions of low values of mass flux and high values of wall heat flux). Practical recommendations are made regarding potential model applications in 3D analyses of SCWRs.

Keywords

Computational Fluid Dynamics, Supercritical Water, Heat Transfer, Vertical Tube, Upward Flow, Validation, PHOENICS software

INTRODUCTION

For more than 40 years, CFD [1] has been increasingly used as a predictive tool in the analyses of supercritical water (SCW) heat transfer in vertical upward and downward tube flows. The standard modern practice is to apply the commercial general-purpose CFD codes (FLUENT, ANSYS-CFX, PHOENICS, etc.) for such analyses. Numerous researchers have assessed FLUENT and ANSYS-CFX for SCW heat transfer modeling with use of different turbulence models and grid settings. Some recent applications of these codes are described in [2-7]. In particular, a detailed review [3] of CFD applications to the modeling of SCW heat transfer in vertical tube flows described the advances and shortcomings in this field. No universal turbulent model has been proposed yet in order to enable researchers to predict accurately SCW heat transfer for a wide range of operating conditions along the whole heated tube length.

In this paper, the PHOENICS CFD software [8] is assessed and validated using the experimental database on SCW heat transfer in a vertical tube with upward flow under operating conditions typical for SCWRs [9-12].

1. MODELING APPROACH

The commercial CFD code, PHOENICS 2014 [8], is used as a framework and a solver to predict SCW heat transfer for vertical upward flow in a tube with an inner diameter of 10 mm and a heated tube length of 4 m under various operating conditions [9-11]. The double-precision solver is employed for better accuracy.

1.1 Numerical Method Description

PHOENICS is a general-purpose commercial CFD code which is applicable to steady or unsteady, one- , two- or three-dimensional turbulent or laminar, single-phase or multi-phase, compressible or incompressible flows using Cartesian, cylindrical-polar or curvilinear coordinates. The code also has a spatial marching integration option to handle parabolic and hyperbolic flows, as well as transonic free jets in the absence of recirculation zones.

The numerical procedure is of the finite-volume type in which the original partial differential equations are converted into algebraic finite-volume equations with the aid of discretization assumptions for the transient, convection, diffusion and source terms. For this purpose, the solution domain is subdivided into a number of control volumes on a mono-block mesh using a conventional staggered-grid approach. All field variables except velocities are stored at the grid nodes, while the velocities themselves are stored at staggered cell-face locations which lie between the nodes.

For complex geometries, PHOENICS by default actually uses a Cartesian cut-cell method named PARSOL which provides an automatic, efficient, and flexible alternative to traditional boundary-fitted grid methods using curvilinear coordinates. The Cartesian cut-cell approach uses a background Cartesian or cylindrical-polar grid for the majority of the flow domain with special treatments being applied to cells which are cut by solid bodies, thus retaining a boundary-conforming grid. Specifically, the method computes the fractional areas and volumes, and employs a collection of special algorithms for computing interfacial areas, evaluating wall shear stresses, and for computing advection and diffusion near solid boundaries, etc.

The finite-volume equations for each variable are derived by integrating the partial differential equations over each control volume. Fully implicit backward differencing is employed for the transient terms, and central differencing is used for the diffusion terms. The convection terms are discretized using hybrid differencing in which the convective terms are approximated by central differences if the cell face Peclet number is less than 2 and otherwise by upwind differencing. At faces where the upwind scheme is used, physical diffusion is omitted altogether. In addition to the upwind and hybrid differencing schemes, PHOENICS is furnished with an extensive set of higher-order convection schemes, which comprise five linear schemes and twelve non-linear schemes.

The integration procedure results in a coupled set of algebraic finite-volume equations which express the value of a variable at a grid node in terms of the values at neighboring grid points and the nodal value at the old time level. The finite-volume equations are solved

iteratively using the SIMPLEST and IPSA algorithms of Spalding, which are embodied in PHOENICS for the solution of single-phase and two-phase flows, respectively. These algorithms are segregated solution methods which employ pressure-velocity coupling to enforce mass conservation by solving a pressure-correction equation and making corrections to the pressure and velocity fields. Multi-phase flows are accommodated using either an Eulerian-Lagrangian method using particle tracking, or an algebraic-slip model.

The default calculation procedure is organized in a slab-by-slab manner in which all dependent variables are solved in turn at the current slab before attention moves to the next higher slab. The slabs are thus visited in turn, from the lowermost to the uppermost, and a complete series of slab visits is referred to as a sweep through the solution domain. For parabolic and hyperbolic calculations, only one such sweep is required, with many iteration cycles at each slab for parabolic cases, and no outflow boundary condition is required because this is an outcome of the solution. For elliptic calculations, many such sweeps are conducted until convergence is attained at the current time level; in addition, the pressure-correction equation is solved in a simultaneous whole-field manner at the end of each sweep. Thereafter the solution proceeds to the next time level where the iterative process is repeated. The option exists to solve each finite-volume equation in a whole-field manner, and this is actually the default when using the automatic convergence control. The default linear equation solver for each finite-volume equation is a modified form of Stone's strongly implicit solver, but the option exists to use a Conjugate Gradient Residuals solver for each equation.

The numerical solution procedure requires appropriate relaxation of the flow variables in order to procure convergence. Two types of relaxation are employed, namely inertial and linear. The former is normally applied to the velocity variables, whereas the latter is applied to all other flow variables, as and when necessary.

The convergence requirement is that for each set of finite-volume equations the sum of the absolute residual sources over the whole solution domain is less than one percent of references quantities based on the total inflow of the variable in question. An additional requirement is that the values of monitored dependent variables at a selected location do not change by more than 0.1 percent between successive iteration cycles. It is also possible to monitor the absolute values of the largest corrections to each variable anywhere in the domain. Once the largest correction falls to zero, or at least a negligible fraction of the value being corrected, then it can be assumed that convergence has been achieved, even if the sum of the residuals has not fallen below the cut-off.

1.2 Details of Customized CFD Model

The cylindrical coordinate system (*X, Y, Z*) is applied in this paper and it is assumed that there are no changes of fluid flow and heat transfer characteristics in the angular *X*-direction. As a result, a simplified axisymmetric 2D formulation is applied (with radial distance, *Y*, and axial distance, *Z*, as independent variables).

The sizes of the computational domain in radial and axial directions are 5 mm and 5 m respectively. The computational domain is extended by 1 m in *Z*-direction upstream in order to generate a fully developed turbulent profile of velocity at the beginning of the heated tube length (at $Z = 1$ m).

Boundary conditions are applied at the inlet (Z = 0.0 m), the outlet (Z = 5 m), the tube wall (Y = 0.005 m) and the flow axis (Y=0), which is treated as a symmetry plane. The inlet temperature, T_{in}, is uniform (320 or 350°C) and the inlet turbulence is specified with a turbulence intensity of 5% and a Prandtl mixing length of 10% of the tube radius. At the inlet, a uniform velocity profile, V_{in}, is specified in accordance with the given mass flux, *G*, and the specified inlet temperature, T_{in}. The outlet of the tube is defined as a fixed pressure boundary. For each modeling case, a uniform heat flux, *q*, is a specified at the heated section of the outer wall (at $Z > 1$ m), and elsewhere the wall is taken as adiabatic.

The following low-Reynolds-number turbulence models available in PHOENICS [8] have been tested: the two-layer k-ε model [13-15], LVEL model [16] and k-ω model [17, 18]. The best results are obtained with the two-layer low-Reynolds-number k-ε model and only these results are described in this paper. This model combines the k-ε model with the one-equation model near the wall [14]. A value of turbulent Prandtl number, Pr_t, equal to 0.86 [19] is selected in all the validation cases. Also, a value of 1.2

is used in the last validation case for comparison purposes. The effect of Pr_t on CFD predictions of SCW heat transfer in upward tube flows was analyzed in detail in [6]. The buoyancy force proportional to the density difference is taken into account in the momentum conservation equation. However, its direct effect on the turbulence field is ignored.

The computational grid is uniform in the axial direction and non-uniform in the radial direction. The radial grid is made significantly finer near the tube wall and it expands towards the axis of the tube: a geometric progression distribution with an expansion ratio of -1.08 is used in all the runs for consistency. The number of radial grid cells varied from 40 to 100 and the final runs are made on grids containing 80x400 and 100x400 cells based on grid sensitivity studies.

The physical properties of supercritical water, like density, viscosity, specific heat at constant pressure and thermal conductivity, vary dramatically approaching pseudo-critical conditions. A fine grid is required to capture these changes accurately. Furthermore, the application of low-Reynolds-number turbulence models requires a fine grid near the tube wall.

The values of non-dimensional distance from the wall surface to the first grid cell face, y^+, are smaller than unity in all the validation runs, which is in accordance with recommendations on the use of low-Reynolds-number turbulence models in previous CFD analyses of SCW heat transfer [2-7]. In particular, y^+ is around 0.1 in most runs. It is calculated as $y^+ = u_* y_1 / \nu$, where u_* is the friction velocity, y_1 is the radial distance from the wall to the first grid node and ν is the local kinematic viscosity. The physical size of the first grid cell, y_1, is kept the same over the heated length in each CFD run, but the non-dimensional distance, y^+, changes along the wall due to change in physical properties of SCW.

The NIST REFPROP software [20] is used to generate the tables of SCW properties (dependencies of density, kinematic viscosity, specific heat at constant pressure, thermal conductivity on local temperature) at a pressure of 24 MPa in the temperature range from 320°C to 600°C. These tables are used to provide a separate Excel table file for each individual property, and these files are then read by the PHOENICS solver at run time. At each computational cell, the above physical properties are calculated using linear interpolation to the local temperature value. For simplicity, the PHOENICS customization tool, INFORM [8], is used for linking the PHOENICS solver with the REFPROP data base instead of using FORTRAN coding and creating a private version of the PHOENICS solver.

2. RESULTS AND DISCISSION

2.1 Experimental Conditions

The CFD model described in the previous section is validated using the experimental data obtained at the State Scientific Center of Russian Federation – Institute for Physics and Power Engineering supercritical-test facility (Obninsk, Russia) [9−11]. This set of data was generated within the operating conditions close to those of SCWRs.

Table 2.1 summarizes the test conditions for each simulated experiment. The main parameters that differentiate the validation cases are the mass flux, G, the wall heat flux, q, and the inlet temperature T_{in}. In all cases, the pressure, P, the inside tube diameter, D, and the heated tube length, L_h, are the same: P = 24 MPa, D = 10 mm, L_h = 4 m.

Table 2.1 Validation cases (P=24 MPa, D = 10 mm, L_h = 4 m)

Case	G, kg/m^{2}s	q, kW/m^2	T_{in}, °C
1	1500	590	350
2	1500	729	320
3	1000	387	320
4	1000	581	350
5	1000	681	350
6	500	141	350
7	500	334	350

2.2 CFD Model Validation

The bulk fluid temperature, the inside tube wall temperature and the heat transfer coefficient are calculated along the heated tube length and compared with experimental data in Cases 1 to 7 listed in Table 2.1. Figures 2.1-2.7 show the comparisons of CFD predictions (solid lines) of bulk fluid temperature, inside tube wall temperature and heat transfer coefficient with

experimental values. In the first six cases considered in this paper (Cases 1 to 6), the agreement is very good along the whole tube length (see Figures 2.1-2.6 for more details). In the last case (Case 7), the quantitative disagreement between the CFD predictions of tube wall temperature and heat transfer coefficient and their experimental values becomes more significant (see Figure 2.7). However, this difference decreases with an increase in Pr_t from 0.86 to 1.2 (see Figures 2.7 and 2.8).

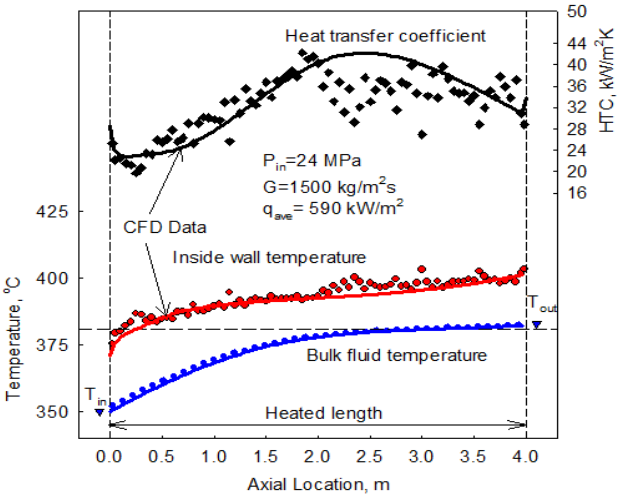

Figure 2.1 Comparison of CFD Predictions (Solid Lines) with Experimental Data in Case 1 (G = 1500 kg/m^{2}s, q = 590 kW/m^2).

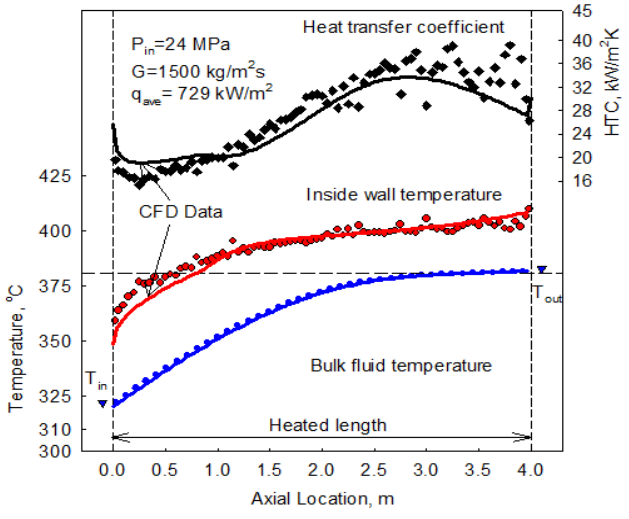

Figure 2.2 Comparison of CFD Predictions (Solid Lines) with Experimental Data in Case 2 (G = 1500 kg/m^{2}s, q = 729 kW/m^2).

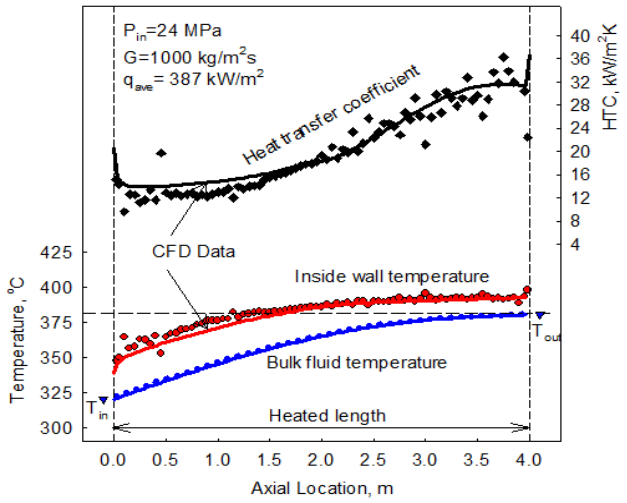

Figure 2.3 Comparison of CFD Predictions (Solid Lines) with Experimental Data in Case 3 (G = 1000 kg/m^{2}s, q = 387 kW/m^2).

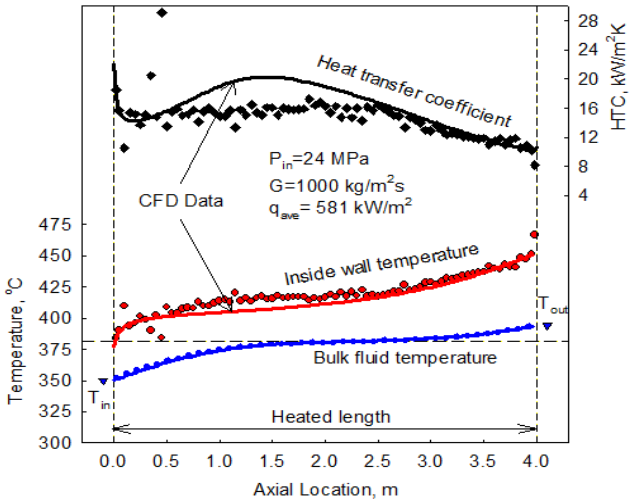

Figure 2.4 Comparison of CFD Predictions (Solid Lines) with Experimental Data in Case 4 (G = 1000 kg/m^{2}s, q = 581 kW/m^2).

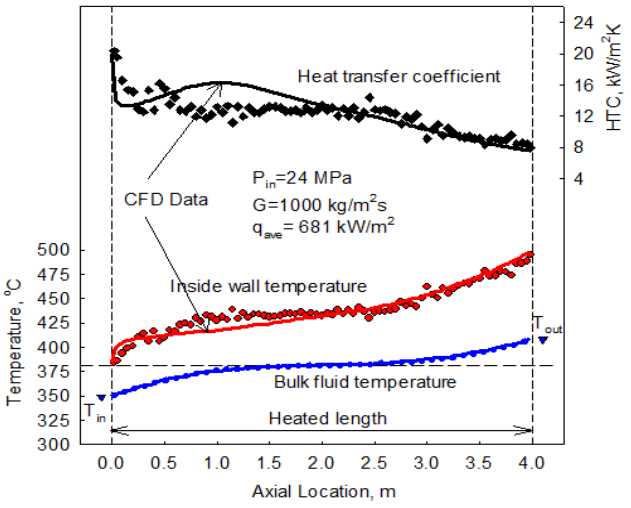

Figure 2.5 Comparison of CFD Predictions (Solid Lines) with Experimental Data in Case 5 (G = 1000 kg/m^{2}s, q = 681 kW/m^2).

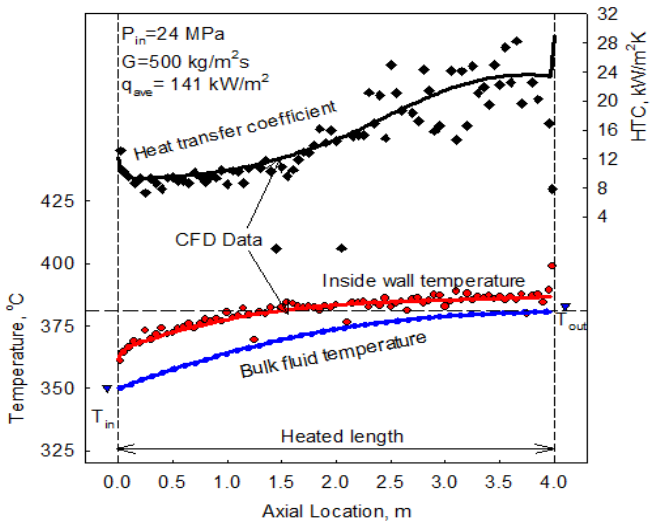

Figure 2.6 Comparison of CFD Predictions (Solid Lines) with Experimental Data in Case 6 (G = 500 kg/m^{2}s, q = 141 kW/m^2).

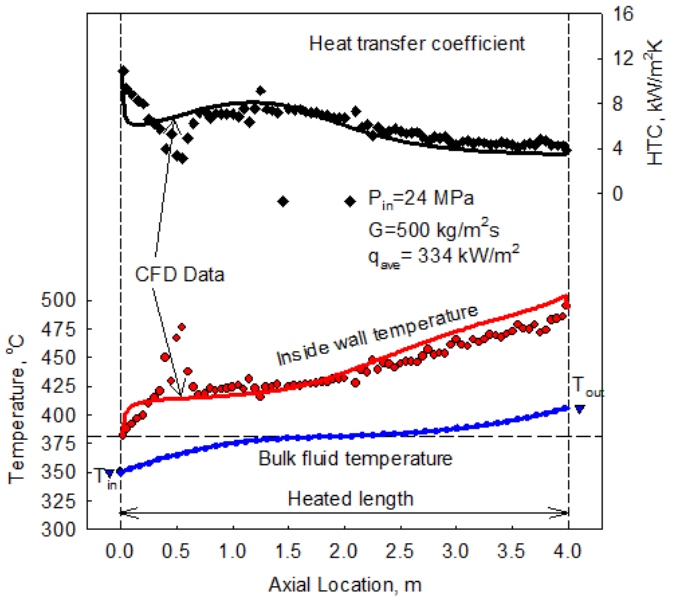

Figure 2.7 Comparison of CFD Predictions (Solid Lines) with Experimental Data in Case 7 (G = 500 kg/m^{2}s, q = 334 kW/m^2) at Pr_t = 0.86.

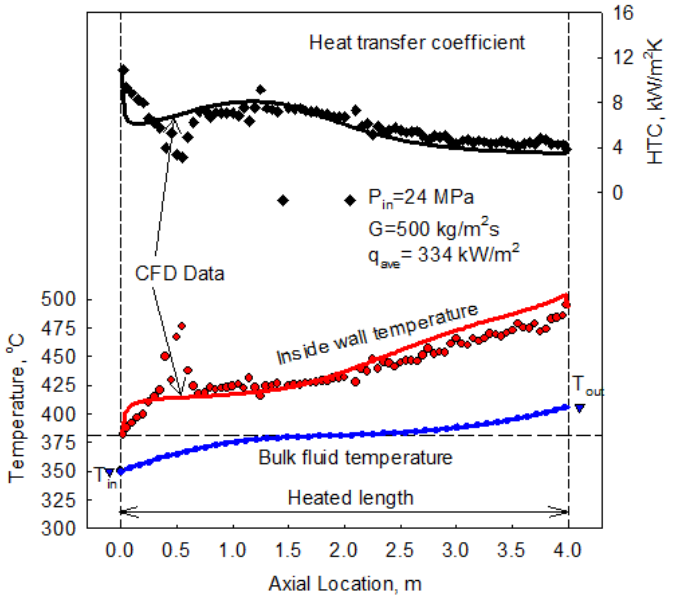

Figure 2.8 Comparison of CFD Predictions (Solid Lines) with Experimental Data in Case 7 (G = 500 kg/m^{2}s, q = 334 kW/m^2) at Pr_t = 1.2.

2.3 Flow Characteristics in Cases 5 and 7

Figure 2.9 shows contour plots of fluid temperature, velocity, density (*DEN1*), laminar kinematic viscosity (*ENUL*), specific heat (*LFCP* in J/kg.K) and laminar Prandtl number ($PRTL=\mu C_p/k$) predicted in Case 5 (T_{in}=350°C, G=1000 kg/(m^{2}s), q=681 kW/m^2).

The origin of cylindrical coordinate system is located in the center of inlet tube section (left bottom corner). A red pencil with yellow end (a probe), which is located at the low right corner of the computational domain, shows the center of outlet section. The values of calculated variables at this probe location and their average values in a plane are shown in the high right corners of the figures. For clarity of presentation, the scale in the Y-direction is increased by a factor of 200 in all the figures.

The dependence of laminar Prandtl number, PRTL, on axial Z-coordinate is non-monotonic: there is a local maximum of about 11.3 in the tube area where the local fluid temperatures are close to the pseudo-critical temperature of 381.2°C and the specific heat (*LFCP*) reaches the maximum value close to 121,930 J/kgK.

In Case 5, the Reynolds number $Re=DV_{in}/\nu_{in}=1.39E+5$; the Grashof number, Gr, defined in this paper as $Gr=(1-\rho_{out}/\rho_{in})gD^3/\nu_{in}^2$, is equal to 6.28E+8; and the value of Richardson number, Ri, which is defined as $Ri=Gr/Re^2=(1-\rho_{out}/\rho_{in})gD/V_{in}^2$, is equal to 0.033. This flow is a mixed convection upward flow in a heated tube, where the buoyancy force caused by density difference becomes important with increase in Ri [21-23]. A detailed review of such flows was provided in [21], where, in particular, it was concluded that the use of low-Reynolds-number turbulence models was required in order to predict accurately the heat transfer characteristics such as tube wall temperature and heat transfer coefficient along the heated tube length.

Due to a large decrease in density (from 621 to about 86 kg/m^3) along the heated tube length, there is a significant acceleration of flow: the velocity increases from an inlet velocity of 1.61 m/s to values up to 8.37 m/s at the tube outlet. Figure 2.10 shows the dependencies of axial velocity on radial distance from the tube axis predicted in Case 5 at different distances from the tube inlet. It is an illustration of significant flow acceleration. However, the effect of buoyancy on radial profiles of axial velocity is not significant in this case (Ri=0.033).

For an increase in Ri, the effect of buoyancy force on fluid velocity and temperature increases and the radial profile of axial velocity starts to have a local maximum between the tube axis and tube wall. This effect was demonstrated in [22] for an ascending air flow in a vertical heated pipe at Re=25,000 and $Gr>10^9$ (Ri>1.6).

Figure 2.11 illustrates the above buoyancy effect predicted in Case 7 (T_{in}=350°C, G=500 kg/(m^{2}s), q=334 kW/m^2). This figure shows the radial profiles of axial velocity calculated at different distances from the tube inlet. The modest local maximums (between the tube axis and tube wall) are predicted for radial profiles of axial velocities at the distances of 2 and 3 m from the tube inlet. It is an indication of the moderate local effect of buoyancy on fluid velocity. In this case, Re=6.94E+4, Gr=6.21E+8 and Ri=0.13.

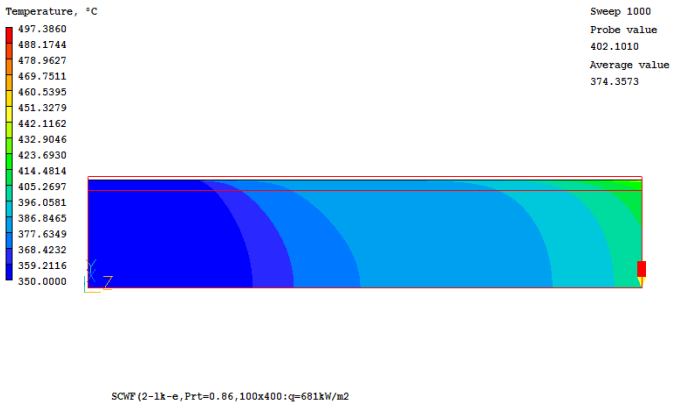

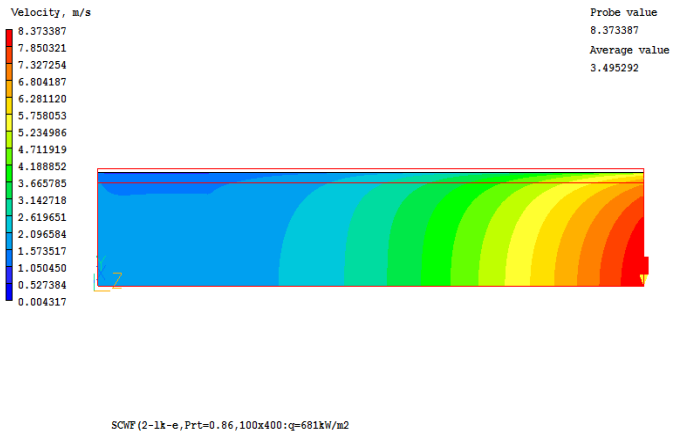

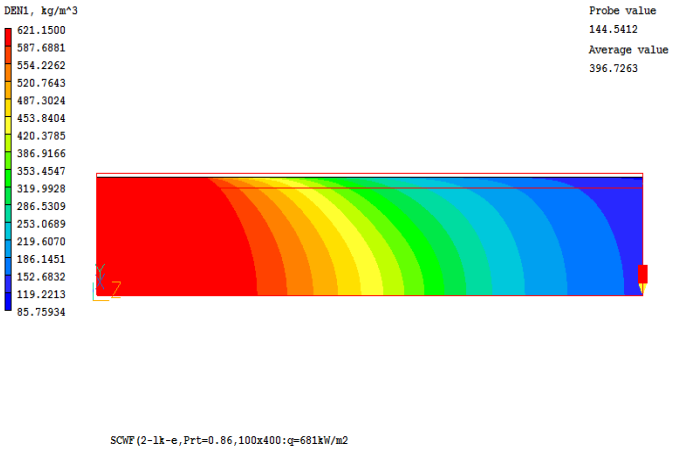

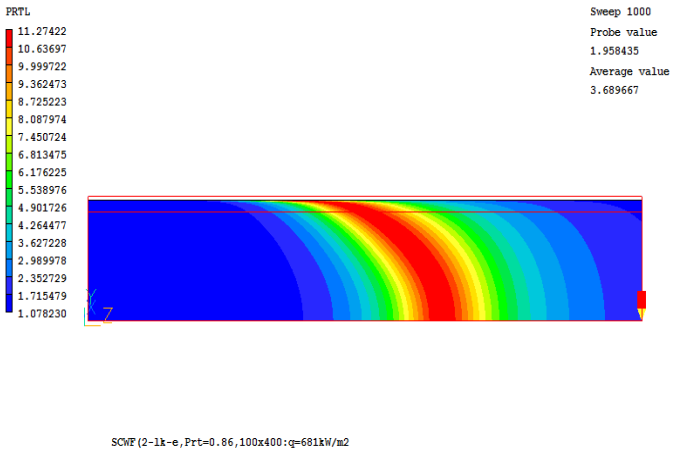

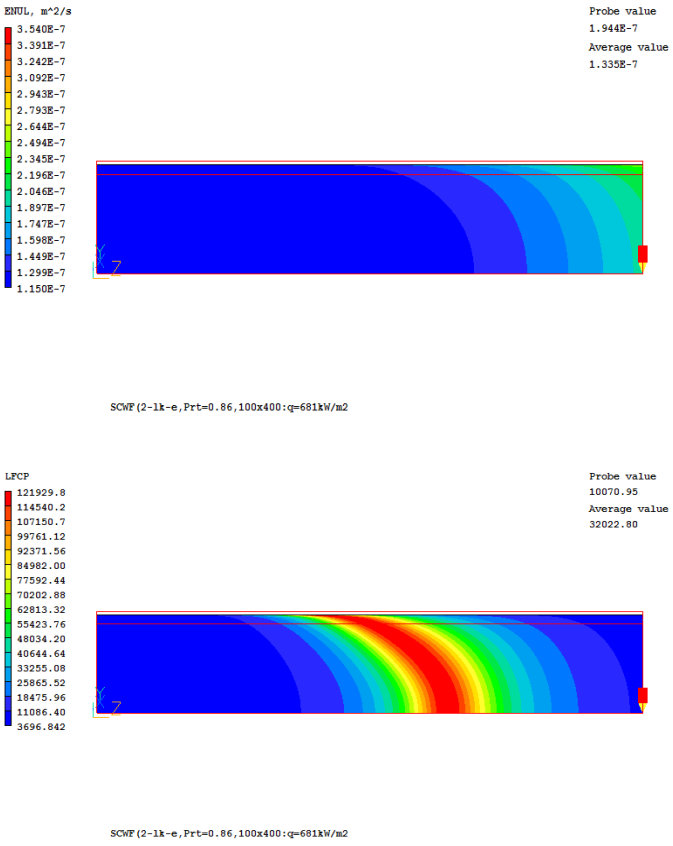

Figure 2.9 Predicted 2D Contours of Temperature, Velocity, Density, Laminar Kinematic Viscosity, Specific Heat and Laminar Prandtl Number in Case 5 (T_{in}=350°C, G=1000 kg/m^{2}s, q=681 kW/m^2).

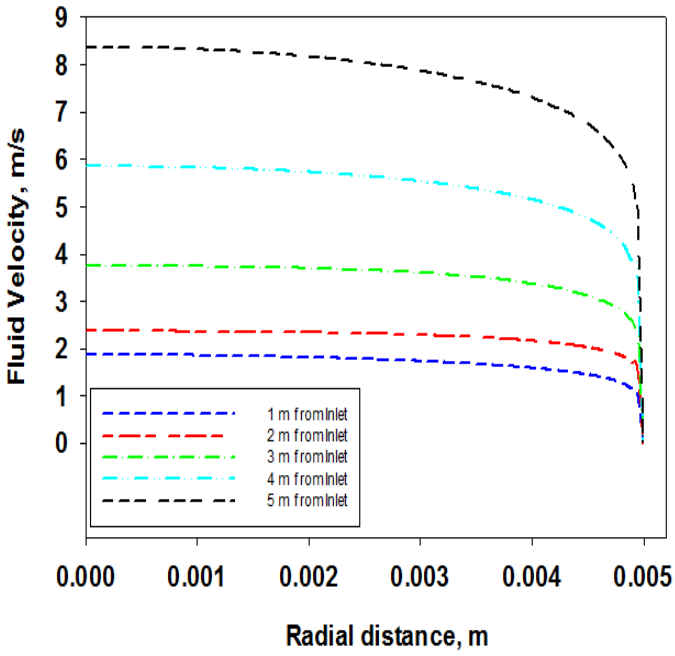

Figure 2.10 Predicted Radial Profiles of Axial Velocity at Various Distances from the Tube Inlet in Case 5 (T_{in}=350°C, G=1000 kg/m^{2}s, q=681 kW/m^2).

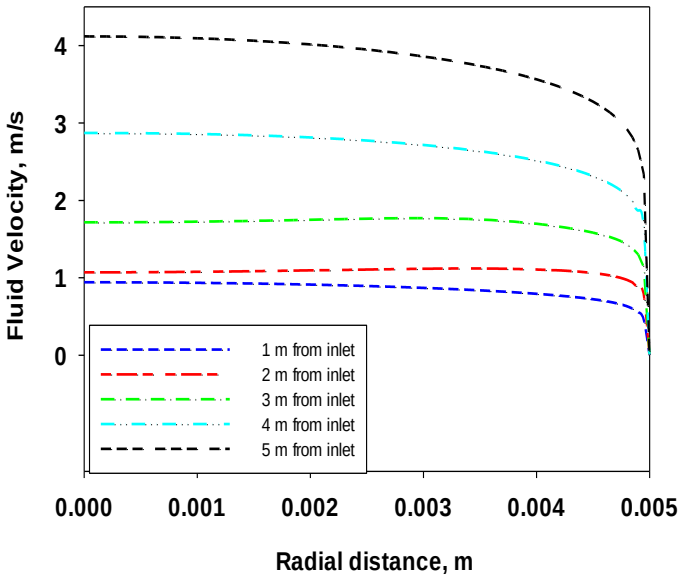

Figure 2.11 Predicted Radial Profiles of Axial Velocity at Various Distances from the Tube Inlet in Case 7 (T_{in}=350°C, G=500 kg/m^{2}s, q=334 kW/m^2).

3. CONCLUSIONS

1. The commercial general-purpose CFD software, PHOENICS 2014, has been customized and validated for modeling the SCW heat transfer in a vertical tube upward flow under the operating conditions typical to SCWRs: a pressure of 24 MPa, an inner tube diameter of 10 mm, an inlet temperature of 320 or 350°C, a heated tube length of 4 m, the three values of mass flux (500, 1000 and 1500 kg/m^{2}s) and various values of wall heat flux (from 141 to 729 kW/m^2).
2. The two-layer low-Reynolds-number k-ε model of turbulence has demonstrated a good performance provided that a turbulent Prandtl number of 0.86 is fixed and the non-dimensional wall distance to the first grid cell face, y^+, is kept below unity. Physical properties of SCW are calculated by using the NIST REFPROP software.
3. The study has shown a good agreement between the CFD predictions and the experimental data on the inside wall temperature and heat transfer coefficient in most validation cases. No model tuning is made for validation purposes within a wide range of flow conditions.
4. However, a further model development is required under the conditions of low values of mass flux, G, and high values of wall heat flux, q, in order to predict accurately the tube wall temperature and heat transfer coefficient (Case 7). In these cases, the buoyancy force becomes significant and an effect of Pr_t on accuracy of CFD predictions of heat transfer increases.
5. The partially validated CFD model of SCW heat transfer in a vertical upward tube flow is recommended for practical 3D geometries under the conditions of moderate effects of buoyancy (moderate values of Richardson number).

NOMENCLATURE

C_p	Specific heat at constant pressure, J/kg·K
D	Inner tube diameter, m
DEN1	Density, kg/m^3
ENUL	Laminar kinematic viscosity, m^2/s
G	Mass flux, kg/m^{2}s
HTC	Heat transfer coefficient, kW/m^2·K
k	Thermal conductivity, W/m·K
L	Length, m
LFCP	Specific heat, J/kgK
P	Pressure, Pa
q	Wall heat flux, kW/m^2
T	Temperature, °C
V	Velocity, m/s

Greek Letters

ν	Laminar kinematic viscosity, m^2/s
ρ	Density, kg/m^3
μ	Laminar dynamic viscosity, Pa s

Dimensionless Numbers

Gr	Grashof number ($(1-\rho_{out}/\rho_{in})gD^3/\nu_{in}^2$)
PRTL	Laminar Prandtl number ($\mu C_p/k$)
Pr_t	Turbulent Prandtl number
Re	Reynolds number (DV_{in}/ν_{in})
Ri	Richardson number (Gr/Re^2)

Subscripts

avg	average
h	heated

in	inlet
out	outlet

Abbreviations

CFD	Computational Fluid Dynamics
SCW	SuperCritical Water
SCWRs	SuperCritical Water Reactors
NIST	National Institute of Standards and Technology

REFERENCES

1. Versteeg, H.K., and Malalasekera, W., 1995. *An introduction to computational fluid dynamics*, Longman, Harlow, UK.
2. Roelofs, F., 2004. CFD analysis of heat transfer to supercritical water flowing vertically upward in a tube. Under the contract of the Netherlands Ministry of Economic Affairs.
3. Cheng, X., Kuang, B., and Yang, Y.H., 2007. Numerical analysis of heat transfer in supercritical water cooled flow channels. Nuclear Engineering and Design, 237, 240-252.
4. Mokry, S., Farah, A., King, K., Gupta, S., Pioro, I., and Kirillov, P., 2009. Development of supercritical water heat-transfer correlation for vertical bare tubes, Proc. International Conference on Nuclear Energy for New Europe 2009, Bled, Slovenia, September 14-17, pp. 210.1-210.13.
5. Vanyukova, G., Kuznetsov, Yu., Loninov, A. et al., 2009. Application of CFD-Code to Calculations of Heat Transfer in a Fuel Bundle of SCW Pressure-Channel Reactor, Proc. 4th Int. Symp. on Supercritical Water-Cooled Reactors, March 8-11, Heidelberg, Germany, Paper No. 28, 9 pages.
6. Jaromin, M. and Anglart, H., 2013. A Numerical Study of the Turbulent Prandtl Number Impact on Heat Transfer to Supercritical Water Flowing Upward under Deteriorated Conditions, Proc. 15th International Topical Meeting on Nuclear Reactor Thermal hydraulics (NURETH-15), May 12–17, Pisa, Italy, paper #134, 14 pages.
7. Farah, A., Harvel, G., and Pioro, I., 2013. Assessment of FLUENT CFD Code as an Analysis Tool for Supercritical-Water Heat-Transfer Applications, Proc. 15th International Topical Meeting on Nuclear Transfer Applications; Proc. 15th International Topical Meeting on Nuclear Reactor Thermal hydraulics (NURETH-15), May 12–17, Pisa, Italy, paper #118, 13 pages.
8. PHOENICS On-Line Information System: www.cham.co.uk/ChmSupport/polis.php.
9. Kirillov, P., Pometko, R., Smirnov, A. et al., 2005. Experimental Study on Heat Transfer to Supercritical Water Flowing in 1- and 4-m-Long Vertical Tubes, Proc. GLOBAL'05, Tsukuba, Japan, Oct. 9-13, Paper No. 518.
10. Pioro, I.L., Kirillov, P.L., Mokry, S.J. and Gospodinov, Y.K., 2008. Supercritical Water Heat Transfer in a Vertical Bare Tube: Normal, Improved and Deteriorated Regimes, Proc. ICAPP'08, Anaheim, CA, USA, June 8-12, Paper #8333, pp. 1843-1852.
11. Gospodinov, Ye., Mokry, S., Pioro, I. and Kirillov, P.L., 2008. Supercritical Water Heat Transfer in a Vertical Bare Tube, Proc. ICONE-16, Orlando, Florida, USA, May 11–15, Paper #48546, 11 pages.
12. Pioro, I. and Duffey, R., 2007. *Heat Transfer and Hydraulic Resistance at Supercritical Pressures in Power Engineering Applications*, ASME Press, New York, NY, USA, 334 pages.
13. Two-layer k-ε model in PHOENICS: http://www.cham.co.uk/phoenics/d_polis/d_enc/turmod/enc_t331.htm.
14. Rodi, W., 1991. Experience with two-layer models combining the k-ε model with a one-equation model near the wall, AIAA-91-0216, 29th Aerospace Sciences Meeting, January 7-10, Reno, Nevada, USA.
15. Norris, L.H., and Reynolds, W.C., 1975. Turbulent channel flow with a moving wavy boundary, Rept. No. FM-10, Stanford University, Mech. Eng. Dept., USA.
16. Agonafer, D., Liao, G-Li., and Spalding, D.B., 1996. The LVEL turbulence model for conjugate heat transfer at low Reynolds numbers, EEP6, ASME International Mechanical Congress and Exposition, Atlanta.

17. Kolmogorov, A.N., 1942. Equations of turbulent motion of an incompressible fluid, Izv. Akad. Nauk SSSR, Ser. Phys., Vol. 6, No. 1-2, p. 56.
18. Wilcox, D.C., 1988. Reassessment of the scale determining equation for advanced turbulence models, AIAA Journal, Vol. 26, No. 11, p. 1299.
19. Malin, M.R., 1987. On the Calculation of Heat Transfer Rates in Fully Turbulent Wall Flows, Appl. Math. Modelling, 11, 281-284.
20. National Institute of Standards and Technology, 2007. NIST Reference Fluid Thermodynamic and Transport Properties-REFPROP. NIST Standard Reference Database 23, Ver. 8.0. Boulder, CO, U.S.: Department of Commerce.
21. Jackson, J.D., Cotton, M.A. and Axcell, B.P., 1989. Studies of Mixed Convection in Vertical Tubes. Int. J. Heat and Fluid Flow, Vol. 10, No. 1, pp. 2-15.
22. Abdelmeguid, A.M., and Spalding, D.B., 1979. Turbulent flow and heat transfer in pipes with buoyancy effects. J. Fluid Mech., 94, 383-400.
23. Hall, W.B., and Jackson, J.D., 1969. Laminarisation of a turbulent pipe flow by buoyancy forces. ASME, Paper No. 69-HT-55.